CSIAM Trans. Life Sci.
doi: 10.4208/csiam-ls.SO-2025-0030

Vol. **x**, No. x, pp. 1-27
xx 2026

The Impact of CD8$^+$ T Cell Exhaustion on HIV Infection Dynamics

Ao Sun[1], Le-Le Fan[1], Ting Guo[2] and Zhi-Peng Qiu[1,*]

[1] *School of Mathematics and Statistics, Nanjing University of Science and Technology, Nanjing 210094, China.*
[2] *Aliyun School of Big Data, Changzhou University, Changzhou 213164, China.*

Received 20 November 2025; Accepted 1 February 2026

Abstract. This study develops a time-varying model to investigate the impact of CD8$^+$ T cell exhaustion on human immunodeficiency virus infection dynamics. For the corresponding autonomous model, the existence and local stability of equilibria are established. Bifurcation analysis reveals complex dynamics, including bistability involving multiple attractors and periodic solutions. Numerical simulations of the time-varying model demonstrate that the progression of CD8$^+$ T cell exhaustion drives an increase in viral load and triggers a bifurcation-induced tipping (B-tipping) point. This leads to a rapid viral surge, which is characteristic of the transition from the asymptomatic stage to AIDS. The non-autonomous system robustly exhibits B-tipping regardless of the CD8$^+$ T cell exhaustion rate (r), which primarily governs the speed of this transition. These findings highlight CD8$^+$ T cell exhaustion as a key driver of post-infection disease progression and elucidate the mechanistic basis for rapid viral surges, thereby providing critical insights into human immunodeficiency virus pathogenesis and the development of therapeutic strategies.

AMS subject classifications: 34C23, 92D25, 34D20
Key words: HIV infection, CD8$^+$ T cell exhaustion, time-varying model, tipping point.

1 Introduction

Human immunodeficiency virus (HIV) remains a major global health threat, having claimed approximately 44.1 million lives by the end of 2024, with an estimated 40.8 million people currently living with HIV. The pandemic continues to pose a severe threat to both public health and socioeconomic development [50]. During HIV infection, activated CD8$^+$ T cells constitute a major component of the antiviral immune response and play a critical role in controlling HIV infection [20]. Elucidating the complex interactions between HIV and CD8$^+$ T cells is therefore crucial. This not only helps elucidate the

*Corresponding author. *Email address:* nustqzp@njust.edu.cn (Z.-P. Qiu)

viral pathogenesis but also paves the way for innovative antiviral therapies and vaccine strategies.

Mathematical models are valuable tools for studying HIV dynamics [19, 20, 32, 34, 38, 39, 44, 45]. In 1996, Nowak and Bangham [34] expanded the basic viral dynamics model through the development of a mathematical framework that incorporated cytotoxic T lymphocyte (CTL) immune responses. Since then, numerous modeling studies have explored the complex relationship between HIV and $CD8^+$ T cells [19,20,32,44,45]. For example, Guo and Qiu [20] developed an HIV dynamics model that incorporated latently infected cells, antiretroviral therapy, cell-free virus infection and cell-to-cell viral transmission, demonstrating that the CTL immune response significantly increase the population of uninfected $CD4^+$ T cells, and effectively reduce both the number of infected cells and the viral load. Ngina *et al.* [32] constructed a model of HIV dynamics, which showed that $CD8^+$ T cells are crucial for suppressing viral replication during the acute infection phase. Graw and Regoes [19] developed a mathematical model to investigate how polyfunctional $CD8^+$ T cell responses, which are characterized by a high frequency of cells able to secrete multiple cytokines simultaneously, influence viral load and disease progression. The results indicate that the strength of the $CD8^+$ T cell response measured by the average number of different effector functions per $CD8^+$ T cell is the best predictor of disease progression.

The aforementioned models have not incorporated the significant impact of $CD8^+$ T cell exhaustion on HIV infection dynamics. In HIV infection, the pathogen cannot be completely eliminated, and $CD8^+$ T cells are subjected to persistent antigenic stimulation and activation. This persistent stimulation causes dysfunction in $CD8^+$ T cells, leading to a hypofunctional state termed T cell exhaustion [8, 21, 41]. Exhausted $CD8^+$ T cells display many features, including reduced effector functions, decreased proliferative capacity, increased expression of inhibitory receptors [4]. This progressive loss of function severely impairs the capacity of $CD8^+$ T cells to control HIV, leading to persistent infection [30]. Therefore, it is important to investigate the impact of $CD8^+$ T cell exhaustion on HIV infection dynamics.

Over the past few decades, numerous studies have employed mathematical modeling to explore $CD8^+$ T cell exhaustion. Wang and Liu [46] proposed an HIV infection model that incorporated cell-mediated immunity and immune impairment, and demonstrated that treatment can shift patients from disease progression to immune control. Regoes *et al.* [37] modeled the immune impairment due to exhaustion as a function of the densities of infected and effector cells to assess its impact on HIV dynamics and evolution, and found that immune impairment elevates viral load and enhances viral diversity and replicative capacity. Conway and Perelson [13] employed Michaelis-Menten saturation terms to model the proliferation and exhaustion of effector cells, and the analysis revealed that viral rebound after discontinuation of antiretroviral therapy (ART) is correlated with the size of the latent viral reservoir and the strength of the CTL response. Based on the model established in [13], Zhang and Ellingson [52] analyzed its dynamic behaviors, concluding that the infected cell death rate and the saturation parameter for

CTL proliferation significantly affect post-treatment control of HIV. These mathematical modeling efforts offer valuable insights into the impact of $CD8^+$ T cell exhaustion on HIV infection dynamics.

In numerous mathematical models for $CD8^+$ T cell exhaustion, parameters associated with the exhaustion features (e.g. the cytotoxic killing rate of infected cells) are constant. However, as the infection progresses, the state of $CD8^+$ T cell exhaustion evolves, suggesting that these parameters may also vary over time. For example, the cytotoxic killing rate of infected cells is likely to decrease over time. To capture these dynamics, we represent parameters associated with $CD8^+$ T cell exhaustion as time-varying functions. In this study, we first introduce a parameter s to quantify the degree of $CD8^+$ T cell exhaustion. Unlike in previous studies, s is not a constant but a time-dependent variable. Parameters related to the exhaustion features are then modeled as functions of s. This formulation allows us to develop a non-autonomous system with time-varying parameters to investigate the impact of $CD8^+$ T cell exhaustion on HIV viral-immune dynamics, thereby providing a novel perspective and methodology for this field of research.

The potential for non-stationary parameter changes to induce tipping points has been widely studied in climate science, ecology, and other fields [17, 27, 33, 40, 49]. A tipping point or critical transition refers to a sudden, substantial, and often irreversible change in a complex system due to small external inputs [35]. To better understand this, Ashwin *et al.* [1, 2] classified tipping points into three types:

(1) Bifurcation-induced tipping (B-tipping) point: A critical transition occurs when the changes in a parameter drive the system through a bifurcation point, leading to a sudden transition from one equilibrium state to another.

(2) Rate-induced tipping (R-tipping) point: This occurs when a parameter changes too rapidly for the system to track its quasi-steady state, causing a large transition, even if the parameter change does not cross a bifurcation point.

(3) Noise-induced tipping (N-tipping) point: System transitions to another stable state due to noise or increased stochasticity.

These tipping mechanisms are crucial in system dynamics and may significantly impact viral-immune dynamics within hosts.

In this study, we employ a non-stationary process $s(t)$ to model the dynamics of $CD8^+$ T cell exhaustion during HIV infection. This formulation yields a non-autonomous system that may experience critical transitions, known as tipping points. In HIV infection, the progression from the asymptomatic stage to AIDS is marked by immune collapse and a rapid surge in viral load. This progression aligns with the theoretical framework of bifurcation-induced (B-tipping) or rate-induced (R-tipping) transitions. Therefore, this paper aims to investigate how non-stationary exhaustion, mediated through $s(t)$, can precipitate such tipping points and influence HIV virus-immune dynamics. Our approach provides novel methodological and conceptual perspectives for deciphering complex dynamics of HIV infection and informing the development of effective therapeutic strategies.

This paper is structured as follows. Section 2 develops a four-dimensional, time-varying mathematical model based on the mechanism of $CD8^+$ T cell exhaustion. Sections 3 and 4 analyze the corresponding fixed-parameter (autonomous) model, establishing the existence and local stability of equilibria, bistability and periodic solutions. Section 5 investigates the impact of $CD8^+$ T cell exhaustion on HIV infection through numerical simulations and identifies associated tipping point phenomena. Finally, Section 6 provides a brief discussion.

2 Model formulation

In this section, we formulate a mathematical model to describe the impact of $CD8^+$ T cell exhaustion on HIV infection dynamics.

During chronic infections, antigen-specific $CD8^+$ T cells undergo a progressive functional decline, characterized by diminished cytokine production and proliferative potential [48,51]. This impairment severely impairs the capacity of $CD8^+$ T cells to control the virus, resulting in persistent infections [30]. Interestingly, terminally exhausted $CD8^+$ T cells retain some cytolytic activity [4]. Evidence that the targeted deletion of exhausted T cells elevates viral load [25,42] confirms that exhausted $CD8^+$ T cells continue to exert a critical, albeit limited, level of immune suppression. Therefore, in mathematical models, $CD8^+$ T cell exhaustion should be characterized by two bounded, dynamic processes: the progressive impairment of cytotoxic capacity and the concurrent loss of proliferative potential, both of which operate within certain physiological limits.

This study simplifies the model proposed in [13] by omitting latent infection and drug treatment, to focus on the impact of $CD8^+$ T cell exhaustion on HIV infection. The model captures $CD8^+$ T cell exhaustion through two key features: impaired effector function and reduced proliferative capacity. Specifically, impaired effector function directly reduces the antiviral efficacy of $CD8^+$ T cells, which is modeled as a decrease in the killing rate of infected cells by effector cells. Reduced proliferative capacity indirectly weakens the host's antiviral response by limiting the expansion of the effector cell population, which is modeled as an increase in the saturation of immune impairment coefficient. Both parameters are defined as functions of exhaustion level, $s(t)$. A schematic diagram of the model is presented in Fig. 1, and the system is described by the following non-autonomous system:

$$\begin{cases} \dfrac{\mathrm{d}T}{\mathrm{d}t} = \lambda - dT - \alpha VT, \\ \dfrac{\mathrm{d}I}{\mathrm{d}t} = \alpha VT - \delta I - m\big(s(t)\big)EI, \\ \dfrac{\mathrm{d}V}{\mathrm{d}t} = pI - cV, \\ \dfrac{\mathrm{d}E}{\mathrm{d}t} = \lambda_E + b_E \dfrac{I}{K_B + I}E - d_E\big(s(t)\big)\dfrac{I}{K_D + I}E - \mu E. \end{cases} \tag{2.1}$$

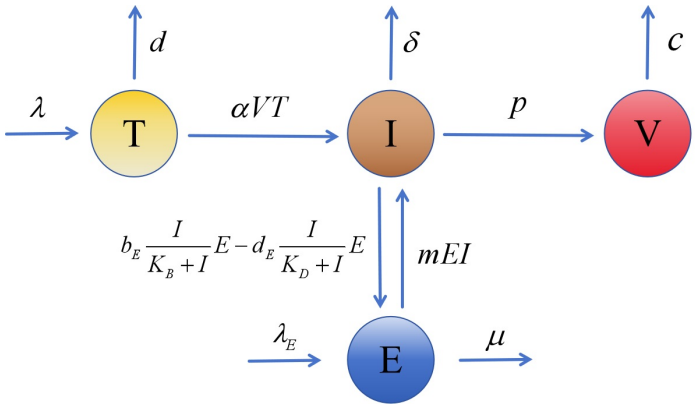

Figure 1: Schematic diagram of model. Variables T, I, V and E represent uninfected CD4$^+$ T cells, infected CD4$^+$ T cells, virus and effector T cells, respectively

In system (2.1), target cells (T) are recruited at a constant rate λ, die at rate d per cell, and become infected with infectivity rate constant α. Infected cells (I) produce virions at rate p per cell and die at the rate of δ by viral cytopathic effects. Virions (V) are cleared at the rate of c. Effector cells (E) kill infected cells under mass action kinetics at the rate of $m(s(t))EI$, where $m(s(t))$ is the killing rate modeled as a decreasing function of the exhaustion level $s(t)$. Effector cells are produced at a constant rate λ_E and undergo natural death at the rate of μ. Upon antigenic stimulation by infected cells, effector cells undergo proliferation as well as immune impairment, both of which are dependent on the density of infected cells. The proliferation of effector cells follows a saturating response, $b_E IE/(K_B+I)$, where b_E is the effector cell proliferation coefficient and K_B is the half-saturation constant. The immune impairment is modeled by the term $d_E(s(t))IE/(K_D+I)$, where $d_E(s(t))$ is an increasing function of the exhaustion level $s(t)$, and K_D ($K_D > K_B$) is the corresponding half-saturation constant.

The parameters $m(s(t))$ and $d_E(s(t))$ are defined as bounded functions that converge to finite limits at the boundaries of their defined intervals and exhibit asymptotically stable behavior. More precisely, we assume $m(s(t)) \in \mathcal{P}(m_{end}, m_{start})$, $d_E(s(t)) \in \mathcal{P}(d_{start}, d_{end})$, where $\mathcal{P}(m_{end}, m_{start}) \subset C^2(\mathbb{R}, (m_{end}, m_{start}))$ and $\mathcal{P}(d_{start}, d_{end}) \subset C^2(\mathbb{R}, (d_{start}, d_{end}))$,

$$\mathcal{P}(m_{end}, m_{start}) = \Big\{ m(s(t)) : m_{end} < m\big(s(t)\big) < m_{start}, \lim_{t\to-\infty} m\big(s(t)\big) = m_{start}, \lim_{t\to+\infty} m\big(s(t)\big) = m_{end}, \lim_{t\to\pm\infty} \frac{\mathrm{d}m\big(s(t)\big)}{\mathrm{d}t} = 0 \Big\}, \tag{2.2}$$

$$\mathcal{P}(d_{start}, d_{end}) = \Big\{ d_E(s(t)) : d_{start} < d_E\big(s(t)\big) < d_{end}, \lim_{t\to-\infty} d_E\big(s(t)\big) = d_{start}, \lim_{t\to+\infty} d_E\big(s(t)\big) = d_{end}, \lim_{t\to\pm\infty} \frac{\mathrm{d}d_E\big(s(t)\big)}{\mathrm{d}t} = 0 \Big\}. \tag{2.3}$$

Here, m_{start} and d_{start} represent the effector cell killing rate and the saturation of immune impairment coefficient at the onset of CD8$^+$ T cell exhaustion, respectively. Conversely, m_{end} and d_{end} correspond to these parameters in the fully exhausted state.

The system can be simplified by considering that viral particles have a significantly shorter average lifespan than infected cells. In viral dynamics, it can be assumed that, compared with the "slow" changes at the level of infected cells, the viral load relatively quickly reaches a quasi-equilibrium level [15, 23]. In a quasi-equilibrium state, the equation $\mathrm{d}V/\mathrm{d}t=0$ holds, yielding $V=pI/c$, which means that V is assumed to be proportional to the changes in the concentration of infected cells I. This allows us to reduce the model to the following three-dimensional system:

$$\begin{cases} \dfrac{\mathrm{d}T}{\mathrm{d}t}=\lambda-dT-\beta IT, \\ \dfrac{\mathrm{d}I}{\mathrm{d}t}=\beta IT-\delta I-m\big(s(t)\big)EI, \\ \dfrac{\mathrm{d}E}{\mathrm{d}t}=\lambda_E+b_E\dfrac{I}{K_B+I}E-d_E\big(s(t)\big)\dfrac{I}{K_D+I}E-\mu E, \end{cases} \tag{2.4}$$

where $\beta=\alpha p/c$.

This study employs system (2.4) to investigate the effect of the non-stationary progression of CD8$^+$ T cell exhaustion on HIV virus-immune dynamics. It also aims to evaluate the significance of CD8$^+$ T cell exhaustion throughout the course of HIV infection, thereby enhancing our understanding of the interaction mechanism among CD8$^+$ T cell exhaustion, HIV infection and the immune system from a mathematical perspective.

3 Local analysis

This section analyzes the dynamics of the autonomous system derived from system (2.4) by fixing all parameters. The corresponding system is as follows:

$$\begin{cases} \dfrac{\mathrm{d}T}{\mathrm{d}t}=\lambda-dT-\beta IT, & \text{(3.1a)} \\ \dfrac{\mathrm{d}I}{\mathrm{d}t}=\beta IT-\delta I-mEI, & \text{(3.1b)} \\ \dfrac{\mathrm{d}E}{\mathrm{d}t}=\lambda_E+b_E\dfrac{I}{K_B+I}E-d_E\dfrac{I}{K_D+I}E-\mu E. & \text{(3.1c)} \end{cases}$$

To ensure that the model captures the progression to AIDS characterized by compromised immunity, we assume $\mu+d_E>b_E$.

In the following, we investigate the existence and local stability of equilibria for system (3.1). We first establish some preliminary results. Based on the biological signifi-

cance, the initial conditions for system (3.1) are assumed to be non-negative: $T(0)\geq 0$, $I(0)\geq 0, E(0)\geq 0$. Let

$$D=\left\{(T,I,E)\in\mathbb{R}^3_+\,\middle|\,0\leq T(t)\leq\frac{\lambda}{a},0\leq I(t)\leq\frac{\lambda}{a},0\leq E(t)\leq\frac{b_E\lambda+mK_B\lambda_E}{mK_B\min\{d,\delta,\mu\}}\right\},$$

where $a=\min\{d,\delta\}$. Then we have the following theorem.

Theorem 3.1. *The region* $\mathbb{R}^3_+=\{(T,I,E)|T(0)\geq 0,I(0)\geq 0,E(0)\geq 0\}$ *is positively invariant, and every trajectory of system* (3.1) *is ultimately attracted to the compact set D.*

Proof. For system (3.1), we have

$$\left.\frac{\mathrm{d}T}{\mathrm{d}t}\right|_{T=0}=\lambda\geq 0,\quad \left.\frac{\mathrm{d}I}{\mathrm{d}t}\right|_{I=0}=0,\quad \left.\frac{\mathrm{d}E}{\mathrm{d}t}\right|_{E=0}=\lambda_E\geq 0.$$

This implies that all trajectories of model (3.1) starting from $\mathbb{R}^3_+$ will enter and stay in this region. From the Eqs. (3.1a) and (3.1b) it follows that

$$\begin{aligned}\frac{\mathrm{d}(T+I)}{\mathrm{d}t}&=\lambda-dT-\delta I-mEI\\&\leq\lambda-\min(d,\delta)(T+I).\end{aligned}$$

Solving this differential inequality gives

$$T(t)+I(t)\leq\frac{\lambda}{\min\{d,\delta\}}+\left(T(0)+I(0)-\frac{\lambda}{\min\{d,\delta\}}\right)e^{-\min\{d,\delta\}t}.$$

Consequently,

$$\limsup_{t\to\infty}T(t),I(t)\leq\frac{\lambda}{\min\{d,\delta\}}.$$

Now, define $z(t)=T(t)+I(t)+nE(t)$, where $n=K_Bm/b_E$. It follows that

$$\begin{aligned}\frac{\mathrm{d}z}{\mathrm{d}t}&\leq\lambda+n\lambda_E-dT-\delta I-\mu nE\\&\leq\lambda+n\lambda_E-\min(d,\delta,\mu)z.\end{aligned}$$

Applying the same method to this inequality yields

$$\limsup_{t\to\infty}z(t)\leq\frac{\lambda+n\lambda_E}{\min\{d,\delta,\mu\}}=\frac{b_E\lambda+mK_B\lambda_E}{b_E\min\{d,\delta,\mu\}}.$$

Since $T(t),I(t)\geq 0$, this bound on $z(t)$ directly implies

$$\limsup_{t\to\infty}E(t)\leq\frac{b_E\lambda+mK_B\lambda_E}{mK_B\min\{d,\delta,\mu\}}.$$

This completes the proof of Theorem 3.1. □

Obviously, system (3.1) always have a unique disease-free equilibrium $\mathscr{E}_0 = (\lambda/d,0,\lambda_E/\mu)$. Using the next generation matrix method, we have

$$\mathbb{F}=\frac{\lambda\beta}{d},\quad \mathbb{V}=\delta+\frac{m\lambda_E}{\mu}.$$

Thus, the basic reproductive number can be expressed by

$$\mathscr{R}_0=\mathbb{F}\mathbb{V}^{-1}=\frac{\lambda\beta\mu}{d(\delta\mu+m\lambda_E)}.$$

In order to classify the equilibria of system (3.1), we begin by presenting some notations that will be used in the following. Define

$$\begin{aligned}
&f(I)=a_0I^3+a_1I^2+a_2I+a_3, \qquad (3.2)\\
&\Delta=4\big(a_1^2-3a_0a_2\big),\\
&\hat{I}=\frac{\lambda\beta-\delta d}{\delta\beta},\\
&I_{L\max}=\frac{-a_1-\sqrt{a_1^2-3a_0a_2}}{3a_0},\\
&I_{L\min}=\frac{-a_1+\sqrt{a_1^2-3a_0a_2}}{3a_0}.
\end{aligned}$$

where

$$\begin{aligned}
&a_0=m\lambda_E\beta+\delta\beta(\mu+d_E-b_E),\\
&a_1=m\lambda_Ed+(\delta\mu+m\lambda_E)\beta(K_B+K_D)+\delta\beta(d_EK_B-b_EK_D)+(\delta d-\lambda\beta)(\mu+d_E-b_E),\\
&a_2=(\delta\mu+m\lambda_E)\beta K_BK_D+(\delta\mu d+m\lambda_Ed-\lambda\beta\mu)(K_B+K_D)+(\delta d-\lambda\beta)(d_EK_B-b_EK_D),\\
&a_3=m\lambda_EdK_BK_D+(\delta d-\lambda\beta)\mu K_BK_D.
\end{aligned}$$

We obtain the following theorem.

Theorem 3.2. *(1) System* (3.1) *always admits a trivial disease-free equilibrium* $\mathscr{E}_0=(\lambda/d,0,\lambda_E/\mu)$. *(2) Suppose that* $\mathscr{R}_0<1$. *Then*

- *(i) if* $\Delta>0, 0<I_{L\min}<\hat{I}$ *and* $f(I_{L\min})<0$, *system* (3.1) *has two positive equilibria, denoted by* $\mathscr{E}_2^*=(T_2^*,I_2^*,E_2^*)$ *and* $\mathscr{E}_3^*=(T_3^*,I_3^*,E_3^*)$ *respectively;*
- *(ii) if* $\Delta>0, 0<I_{L\min}<\hat{I}$ *and* $f(I_{L\min})=0$, *system* (3.1) *has only one positive equilibrium, denoted by* $\mathscr{E}_{2,3}^*=(T_{2,3}^*,I_{2,3}^*,E_{2,3}^*)$;
- *(iii) otherwise, system* (3.1) *has no positive equilibrium.*

(3) Suppose that $\mathscr{R}_0>1$. *Then*

- *(i) if* $\Delta>0, 0<I_{L\max},I_{L\min}<\hat{I}, f(I_{L\max})>0$ *and* $f(I_{L\min})<0$, *system* (3.1) *has three positive equilibria, denoted by* $\mathscr{E}_1^*=(T_1^*,I_1^*,E_1^*)\mathscr{E}_2^*=(T_2^*,I_2^*,E_2^*)$ *and* $\mathscr{E}_3^*=(T_3^*,I_3^*,E_3^*)$ *respectively;*

(ii) if $\Delta>0, 0<I_{L\max}$, $I_{L\min}<\hat{I}$, *and* $f(I_{L\max})=0$, *system* (3.1) *has two positive equilibria, denoted by* $\mathscr{E}_{1,2}^*=(T_{1,2}^*,I_{1,2}^*,E_{1,2}^*)$ *and* $\mathscr{E}_3^*=(T_3^*,I_3^*,E_3^*)$ *respectively;*

(iii) if $\Delta>0, 0<I_{L\max}$, $I_{L\min}<\hat{I}$, *and* $f(I_{L\min})=0$, *system* (3.1) *has two positive equilibria, denoted by* $\mathscr{E}_1^*=(T_1^*,I_1^*,E_1^*)$ *and* $\mathscr{E}_{2,3}^*=(T_{2,3}^*,I_{2,3}^*,E_{2,3}^*)$ *respectively;*

(iv) otherwise, system (3.1) *has only one positive equilibrium, denoted by* $\mathscr{E}_1^*=(T_1^*,I_1^*,E_1^*)$ *or* $\mathscr{E}_3^*=(T_3^*,I_3^*,E_3^*)$.

Proof. Any equilibrium point of system (3.1) satisfy the following equalities:

$$\begin{cases} \lambda-dT-\beta IT=0, & \text{(3.3a)}\\ \beta IT-\delta I-mEI=0, & \text{(3.3b)}\\ \lambda_E+b_E\dfrac{I}{K_B+I}E-d_E\dfrac{I}{K_D+I}E-\mu E=0. & \text{(3.3c)} \end{cases}$$

From the Eqs. (3.3a) and (3.3b), it follows that

$$\begin{cases} T=\dfrac{\lambda}{d+\beta I},\\ E=\dfrac{1}{m}\left(\dfrac{\lambda\beta}{d+\beta I}-\delta\right). \end{cases} \tag{3.4}$$

Substituting (3.4) into the Eq. (3.3c) yields

$$f(I)=0. \tag{3.5}$$

We can see that $E>0$ if and only if $I\le\hat{I}$. To classify the equilibria of system (3.1), it is sufficient to investigate the roots of Eq. (3.5) in the interval $(0,\hat{I})$. Direct calculation yields that

$$\begin{aligned} f(0)&=\lambda\beta\mu K_BK_D\left(\frac{1}{\mathscr{R}_0}-1\right),\\ f(\hat{I})&=\frac{m\lambda\lambda_E}{\delta^3\beta}(\delta\beta K_B+\lambda\beta-\delta d)(\delta\beta K_D+\lambda\beta-\delta d)>0. \end{aligned}$$

Since $\mu+d_E>b_E$, we have $a_0>0$. Consequently, $f(I)$ satisfies $\lim_{I\to-\infty}f(I)=-\infty$ and $\lim_{I\to+\infty}f(I)=+\infty$. Furthermore, if $\Delta>0$, $f(I)$ has two critical points, denoted by $I_{L_{\max}}$ and $I_{L_{\min}}$, corresponding to a local maximum and a local minimum, respectively. We now consider two cases.

Case 1. $\mathscr{R}_0<1$. In this case, $\lim_{I\to-\infty}f(I)=-\infty$ and $f(0)>0$, thus Eq. (3.5) admits at least one root in the interval $(-\infty,0)$. Consequently, Eq. (3.5) may have $0,1$, or 2 roots in the interval $(0,\hat{I})$. Moreover,

(i) if $\Delta>0, 0<I_{L_{\min}}<\hat{I}$, and $f(I_{L_{\min}})<0$, it follows that Eq. (3.5) has two roots I_2^* and I_3^* in $(0,\hat{I})$ (see Fig. 2(a)). Therefore, system (3.1) admits two positive equilibria, denoted by $\mathscr{E}_2^*=(T_2^*,I_2^*,E_2^*)$ and $\mathscr{E}_3^*=(T_3^*,I_3^*,E_3^*)$;

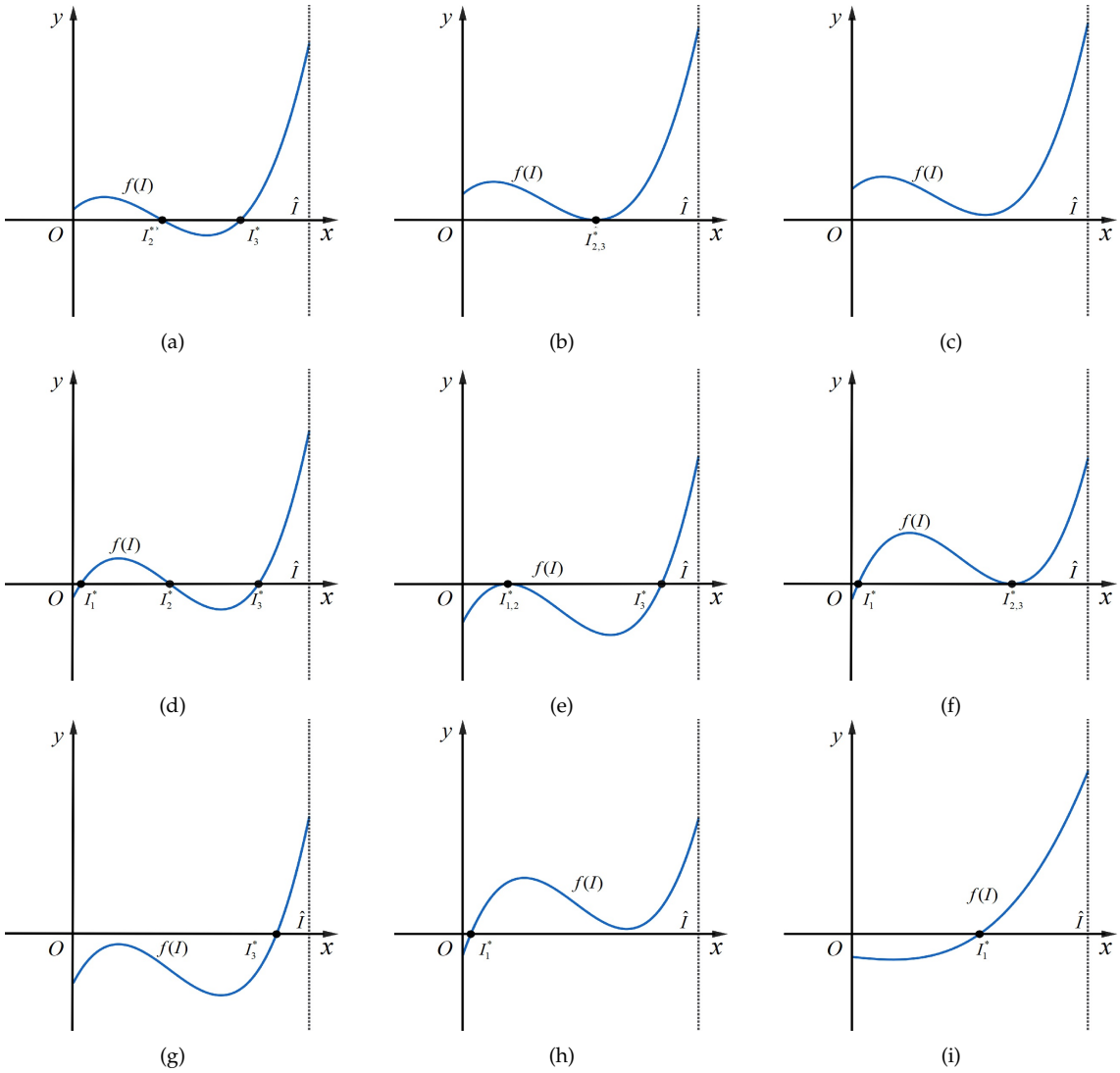

Figure 2: Graphs for the functions $f(I)$ in the interval $(0,\hat{I})$.

(ii) if $\Delta>0, 0<I_{L_{\min}}<\hat{I}$, and $f(I_{L_{\min}})=0$, Eq. (3.5) exhibits a double root $I^*_{2,3}$ in $(0,\hat{I})$ (see Fig. 2(b)). In this case, system (3.1) possesses a unique positive equilibrium, denoted by $\mathscr{E}^*_{2,3}=(T^*_{2,3},I^*_{2,3},E^*_{2,3})$;

(iii) otherwise, no roots of Eq. (3.5) exist in $(0,\hat{I})$ (see Fig. 2(c)), and system (3.1) has no positive equilibrium.

Case 2. $\mathscr{R}_0>1$. In this case, $\lim_{I\to-\infty}f(I)=-\infty$ and $f(0)<0$, implying that Eq. (3.5) admits at most two roots in $(-\infty,0)$. Consequently, Eq. (3.5) possesses at least one and at most three roots in the interval $(0,\hat{I})$. Moreover,

(i) if $\Delta>0, 0<I_{L_{\max}} I_{L_{\min}}<\hat{I}, f(I_{L_{\max}})>0$, and $f(I_{L_{\min}})<0$, Eq. (3.5) has three roots I_1^*, I_2^* and I_3^* in $(0,\hat{I})$ (see Fig. 2(d)). Therefore, system (3.1) admits three positive equilibria: $\mathscr{E}_1^*=(T_1^*,I_1^*,E_1^*), \mathscr{E}_2^*=(T_2^*,I_2^*,E_2^*)$, and $\mathscr{E}_3^*=(T_3^*,I_3^*,E_3^*)$;

(ii) if $\Delta>0$, $0<I_{L_{\max}}, I_{L_{\min}}<\hat{I}$, and $f(I_{L_{\max}})=0$, Eq. (3.5) exhibits a double root $I_{1,2}^*$ and a simple root I_3^* in $(0,\hat{I})$ (see Fig. 2(e)). In this case, system (3.1) has two positive equilibria: $\mathscr{E}_{1,2}^*=(T_{1,2}^*,I_{1,2}^*,E_{1,2}^*)$ and $\mathscr{E}_3^*=(T_3^*,I_3^*,E_3^*)$;

(iii) if $\Delta>0, 0<I_{L_{\max}}, I_{L_{\min}}<\hat{I}$, and $f(I_{L_{\min}})=0$, Eq. (3.5) contains a simple root I_1^* and a double root $I_{2,3}^*$ in $(0,\hat{I})$ (see Fig. 2(f)). Here, system (3.1) has two positive equilibria: $\mathscr{E}_1^*=(T_1^*,I_1^*,E_1^*)$ and $\mathscr{E}_{2,3}^*=(T_{2,3}^*,I_{2,3}^*,E_{2,3}^*)$;

(iv) otherwise, Eq. (3.5) has exactly one root I_1^* or I_3^* in $(0,\hat{I})$ (see Figs. 2(g)-2(i)), and system (3.1) possesses a unique positive equilibrium $\mathscr{E}_1^*=(T_1^*,I_1^*,E_1^*)$ or $\mathscr{E}_3^*=(T_3^*,I_3^*,E_3^*)$.

This completes the proof of theorem. □

We now analyze the stability of the equilibria in system (3.1). The stability of the unique disease-free equilibrium $\mathscr{E}_0=(\lambda/d,0,\lambda_E/\mu)$ is determined as follows.

Theorem 3.3. *For system* (3.1)*, the disease-free equilibrium* $\mathscr{E}_0=(\lambda/d,0,\lambda_E/\mu)$ *is locally asymptotically stable if* $\mathscr{R}_0<1$*, and unstable if* $\mathscr{R}_0>1$*.*

Proof. The Jacobian matrix at the equilibrium $\mathscr{E}_0=(\lambda/d,0,\lambda_E/\mu)$ is

$$J(\mathscr{E}_0)=\begin{pmatrix} -d & -\dfrac{\lambda\beta}{d} & 0 \\ 0 & \dfrac{\lambda\beta}{d}-\delta-\dfrac{m\lambda_E}{\mu} & 0 \\ 0 & \dfrac{\lambda_E}{\mu}\left(\dfrac{b_E}{K_B}-\dfrac{d_E}{K_D}\right) & -\mu \end{pmatrix}.$$

The eigenvalues of $J(\mathscr{E}_0)$ are readily obtained as $-d$, $\lambda\beta/d-(\delta\mu+m\lambda_E)/\mu$, and $-\mu$. Therefore, $\mathscr{E}_0$ is stable if and only if $\lambda\beta/d-(\delta\mu+m\lambda_E)/\mu<0$ (i.e. $\mathscr{R}_0<1$) and unstable if $\lambda\beta/d-(\delta\mu+m\lambda_E)/\mu>0$ (i.e. $\mathscr{R}_0>1$). This completes the proof of theorem. □

We now analyze the stability of the positive equilibria in system (3.1).

Theorem 3.4.

(1) If the positive equilibrium $\mathscr{E}_1^*=(T_1^*,I_1^*,E_1^*)$ *exists (except for the case where* $\Delta=0$ *and* $I_1^*=-a_1/(3a_0)$*, then it is either locally asymptotically stable, or the dimension of its unstable manifold or center manifold is even.*

(2) If the positive equilibrium $\mathscr{E}_1^*=(T_1^*,I_1^*,E_1^*)$ *exists, and* $\Delta=0$*,* $I_1^*=-a_1/(3a_0)$*, then it has at least one dimensional central manifold and at most one dimensional unstable manifold.*

(3) If the positive equilibrium $\mathscr{E}_2^*=(T_2^*,I_2^*,E_2^*)$ *exists, then it is unstable.*

(4) If the positive equilibrium $\mathscr{E}_3^*=(T_3^*,I_3^*,E_3^*)$ exists, then it is either locally asymptotically stable, or the dimension of its unstable manifold or center manifold is even.

(5) If the positive equilibrium $\mathscr{E}_{1,2}^*=(T_{1,2}^*,I_{1,2}^*,E_{1,2}^*)$ exists, then it has at least one dimensional central manifold and at most one dimensional unstable manifold.

(6) If the positive equilibrium $\mathscr{E}_{2,3}^*=(T_{2,3}^*,I_{2,3}^*,E_{2,3}^*)$ exists, then it has at least one dimensional central manifold and at most one dimensional unstable manifold.

Proof. Let $\mathscr{E}^*(T^*,I^*,E^*)$ be a positive equilibrium of system (3.1). The Jacobian matrix at $\mathscr{E}^*$ is

$$J(\mathscr{E}^*)=\begin{pmatrix} -d-\beta I^* & -\beta T^* & 0 \\ \beta I^* & 0 & -mI^* \\ 0 & -\dfrac{E^*g(I^*)}{(K_B+I^*)^2(K_D+I^*)^2} & -\dfrac{\lambda_E}{E^*} \end{pmatrix},$$

where

$$g(I^*)=(d_EK_D-b_EK_B){I^*}^2+2K_BK_D(d_E-b_E)I^*+K_BK_D(d_EK_B-b_EK_D).$$

Following the approach in [16], we find

$$\det\big(J(\mathscr{E}^*)\big)=-\frac{I^*}{(K_B+I*)(K_D+I^*)}f'(I^*),$$

where $f(I)$ has been defined in (3.2).

Let $\xi_i(\mathscr{E}^*)$ for i=1,2,3 be the eigenvalues of $J(\mathscr{E}^*)$, ordered such that $\Re\xi_i(\mathscr{E}^*)\leqslant\Re\xi_j(\mathscr{E}^*)$ for $i<j$. From the properties of the eigenvalues, it follows that

$$\begin{aligned}&\textstyle\sum_{i=1}^3\xi_i(\mathscr{E}^*)=\mathrm{tr}\big(J(\mathscr{E}^*)\big)=-\dfrac{\lambda_E}{E^*}-\dfrac{\lambda}{T^*}<0,\\ &\textstyle\prod_{i=1}^3\xi_i(\mathscr{E}^*)=\det\big(J(\mathscr{E}^*)\big)=-\dfrac{I^*}{(K_B+I*)(K_D+I^*)}f'(I^*).\end{aligned}$$

To analyze the stability of the positive equilibria, we first examine $f'(I)$. Note that $f'(I)$ is a convex quadratic function since $a_0>0$. The sign structure of $f'(I)$ is characterized as follows:

(1) If $\Delta>0$, then $f'(I)$ has two distinct real roots $I_{L_{\max}}$ and $I_{L_{\min}}$ (with $I_{L_{\max}}<I_{L_{\min}}$), and

$$\begin{aligned}&f'(I)<0, \quad I\in(I_{L_{\max}},I_{L_{\min}}),\\ &f'(I)=0, \quad I=I_{L_{\max}} \text{ or } I_{L_{\min}},\\ &f'(I)>0, \quad I\in(-\infty,I_{L_{\max}})\cup(I_{L_{\min}},+\infty).\end{aligned}$$

(2) If $\Delta=0$, then $f'(I)=0$ if and only if $I=-a_1/(3a_0)$. In the other cases, $f'(I)>0$.

(3) If $\Delta<0$, then $f'(I)>0$ holds.

We now analyze the stability of the positive equilibria based on these properties.

(1) Suppose that the positive equilibrium $\mathscr{E}_1^*$ exists (except for the case where $\Delta=0$ and $I_1^*=-a_1/(3a_0)$). We have

$$\sum_{i=1}^3 \xi_i(\mathscr{E}_1^*)=\mathrm{tr}\big(J(\mathscr{E}_1^*)\big)=-\frac{\lambda_E}{E_1^*}-\frac{\lambda}{T_1^*}<0,$$
$$\prod_{i=1}^3 \xi_i(\mathscr{E}_1^*)=\det\big(J(\mathscr{E}_1^*)\big)=-\frac{I_1^*}{(K_B+I_1^*)(K_D+I_1^*)}f'(I_1^*)<0.$$

This implies that the number of the eigenvalues with nonnegative real parts of the matrix $J(\mathscr{E}_1^*)$ are zero or even. Thus, the positive equilibrium $\mathscr{E}_1^*$ is locally asymptotically stable or the dimension of its unstable and center manifold are even.

(2) Suppose that the positive equilibrium $\mathscr{E}_1^*$ exists, and $\Delta=0, I_1^*=-a_1/(3a_0)$. We have

$$\sum_{i=1}^3 \xi_i(\mathscr{E}_1^*)=\mathrm{tr}\big(J(\mathscr{E}_1^*)\big)=-\frac{\lambda_E}{E_1^*}-\frac{\lambda}{T_1^*}<0,$$
$$\prod_{i=1}^3 \xi_i(\mathscr{E}_1^*)=\det\big(J(\mathscr{E}_1^*)\big)=-\frac{I_1^*}{(K_B+I_1^*)(K_D+I_1^*)}f'(I_1^*)=0.$$

This implies that the matrix $J(\mathscr{E}_1^*)$ has at least one zero eigenvalue and at least one eigenvalue with negative real parts. Thus, the positive equilibrium $\mathscr{E}_1^*$ has at least one dimensional central manifold and at most one dimensional unstable manifold.

(3) Suppose that the positive equilibrium $\mathscr{E}_2^*$ exists. We have

$$\sum_{i=1}^3 \xi_i(\mathscr{E}_2^*)=\mathrm{tr}\big(J(\mathscr{E}_2^*)\big)=-\frac{\lambda_E}{E_2^*}-\frac{\lambda}{T_2^*}<0,$$
$$\prod_{i=1}^3 \xi_i(\mathscr{E}_2^*)=\det\big(J(\mathscr{E}_2^*)\big)=-\frac{I_2^*}{(K_B+I_2^*)(K_D+I_2^*)}f'(I_2^*)>0.$$

This implies that the number of the eigenvalues with positive real parts of the matrix $J(\mathscr{E}_2^*)$ are odd. Thus, the positive equilibrium $\mathscr{E}_2^*$ is always unstable and the dimension of its unstable manifold is always odd.

(4) Suppose that the positive equilibrium $\mathscr{E}_3^*$ exists. We have

$$\sum_{i=1}^3 \xi_i(\mathscr{E}_3^*)=\mathrm{tr}\big(J(\mathscr{E}_3^*)\big)=-\frac{\lambda_E}{E_3^*}-\frac{\lambda}{T_3^*}<0,$$
$$\prod_{i=1}^3 \xi_i(\mathscr{E}_3^*)=\det\big(J(\mathscr{E}_3^*)\big)=-\frac{I_3^*}{(K_B+I_3^*)(K_D+I_3^*)}f'(I_3^*)<0.$$

This implies that the number of the eigenvalues with nonnegative real parts of the matrix $J(\mathscr{E}_3^*)$ are zero or even. Thus, the positive equilibrium $\mathscr{E}_3^*$ is locally asymptotically stable or the dimension of its unstable and center manifold are even.

(5) Suppose that the positive equilibrium $\mathscr{E}^*_{1,2}$ exists. We have

$$\sum_{i=1}^{3}\xi_i(\mathscr{E}^*_{1,2})=\mathrm{tr}\big(J(\mathscr{E}^*_{1,2})\big)=-\frac{\lambda_E}{E^*_{1,2}}-\frac{\lambda}{T^*_{1,2}}<0,$$
$$\prod_{i=1}^{3}\xi_i(\mathscr{E}^*_{1,2})=\det\big(J(\mathscr{E}^*_{1,2})\big)=-\frac{I^*_{1,2}}{(K_B+I^*_{1,2})(K_D+I^*_{1,2})}f'(I^*_{1,2})=0.$$

This implies that the matrix $J(\mathscr{E}^*_{1,2})$ has at least one zero eigenvalue and at least one eigenvalue with negative real parts. Thus, the positive equilibrium $\mathscr{E}^*_{1,2}$ has at least one dimensional central manifold and at most one dimensional unstable manifold.

(6) Suppose that the positive equilibrium $\mathscr{E}^*_{2,3}$ exists. We have

$$\sum_{i=1}^{3}\xi_i(\mathscr{E}^*_{2,3})=\mathrm{tr}\big(J(\mathscr{E}^*_{2,3})\big)=-\frac{\lambda_E}{E^*_{2,3}}-\frac{\lambda}{T^*_{2,3}}<0,$$
$$\prod_{i=1}^{3}\xi_i(\mathscr{E}^*_{2,3})=\det\big(J(\mathscr{E}^*_{2,3})\big)=-\frac{I^*_{2,3}}{(K_B+I^*_{2,3})(K_D+I^*_{2,3})}f'(I^*_{2,3})=0.$$

This implies that the matrix $J(\mathscr{E}^*_{2,3})$ has at least one zero eigenvalue and at least one eigenvalue with negative real parts. Thus, the positive equilibrium $\mathscr{E}^*_{2,3}$ has at least one dimensional central manifold and at most one dimensional unstable manifold.

This completes the proof of Theorem 3.4. □

4 Complex dynamics

In this section, the bifurcation of system (3.1) is analyzed to investigate its complex dynamics.

For our numerical analysis, we vary the parameters m (effector cell killing rate) and d_E (saturation of immune impairment coefficient), with all others kept constant. All parameter values used in the simulations are summarized in Table 1.

Bifurcation diagrams shown in Figs. 3 and 4 are generated using the parameter values given in Table 1. Fig. 3 presents a bifurcation diagram for system (3.1), with m as the bifurcation parameter and a fixed value of $d_E=5$. From Fig. 3, if $m<m^{BP,2}$, the unique positive equilibrium $\mathscr{E}^*_3$ is locally asymptotically stable. If $m^{BP,2}<m<m^{BP,1}$, there are three positive equilibria corresponding to $\mathscr{E}^*_1$, $\mathscr{E}^*_2$, and $\mathscr{E}^*_3$, respectively. The equilibria $\mathscr{E}^*_1$ and $\mathscr{E}^*_3$ are stable, and $\mathscr{E}^*_2$ is unstable. When $m^{BP,1}<m<m^{BP,3}$, system (3.1) exhibits two positive equilibria $\mathscr{E}^*_2$ and $\mathscr{E}^*_3$. The equilibrium $\mathscr{E}^*_2$ is always unstable. As m increases through m^H, the equilibrium $\mathscr{E}^*_3$ undergoes a Hopf bifurcation, transitioning from stability ($m<m^H$) to instability ($m^H<m$). Since the first Lyapunov coefficient of system (3.1) at $m=m^H$ is -1.225×10^{-4}, a supercritical Hopf bifurcation occurs at $m=m^H$ for system (3.1). This implies the appearance of a stable limit cycle as m passes through m^H.

Table 1: Parameter values used in simulations.

Variables	Description	Value	Ref
λ	Target cell production	$10^4\,\text{cells/mL/day}$	[9]
d	Target cell death rate	$0.01\,\text{day}^{-1}$	[9]
α	Mass-action infectivity	$1.5\times10^{-8}\,\text{mL/day}$	[13]
δ	infected cell death rate	$1\,\text{day}^{-1}$	[29]
m	Effector cell killing rate	–	–
p	Viral production rate	$2000\,\text{day}^{-1}$	[13]
c	Virion clearance rate	$23\,\text{day}^{-1}$	[13]
λ_E	Effector cell production rate	$1\,\text{cell/mL/day}$	[13]
b_E	Effector cell proliferation coefficient	$4\,\text{day}^{-1}$	[10,52]
K_B	Effector cell production Hill function scaling	$2\,\text{cells/mL}$	[10,52]
d_E	Saturation of immune impairment coefficient	–	–
K_D	Saturation of immune impairment Hill function scaling	$5\,\text{cells/mL}$	[10,52]
μ	Effector cell loss rate	$1.5\,\text{day}^{-1}$	[52]

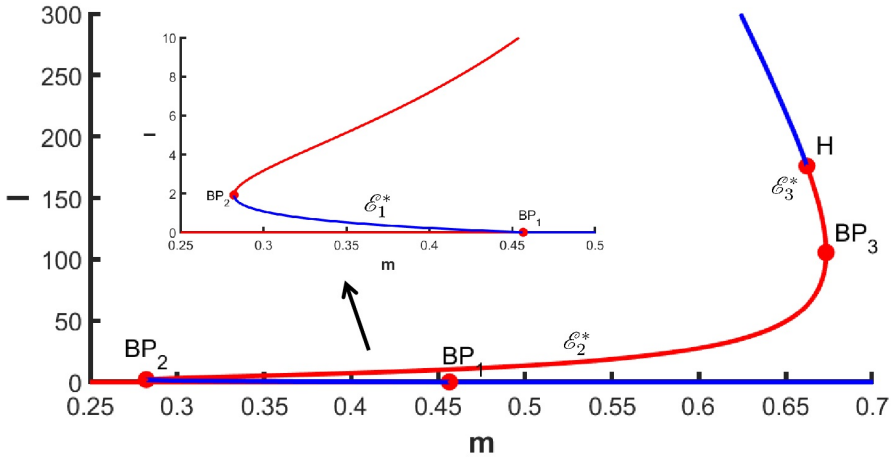

Figure 3: Bifurcation diagram with m as the bifurcation parameter. The value of d_E is chosen to be $d_E=5$. All other parameter values are listed in Table 1. BP denotes branch point and H denotes Hopf bifurcation point. Blue lines represent stable equilibrium, while red lines represent unstable equilibrium. The numerical simulation shows three branch points and one Hopf bifurcation point at $m^{BP_2}=0.282, m^{BP_1}=0.457, m^H=0.662$, and $m^{BP_3}=0.673$, respectively, as m increases. The first Lyapunov coefficients of system (3.1) at $m=m^H$ is -1.225×10^{-4}.

For $m>m^{BP,3}$, system (3.1) has no positive equilibrium. These dynamical behaviors are illustrated in Fig. 5.

Fig. 4 presents a bifurcation diagram in the (d_E,I)-parameter space with fixed m=0.42. It shows that as d_E increases, system (3.1) exhibits sequential bifurcations: two branch

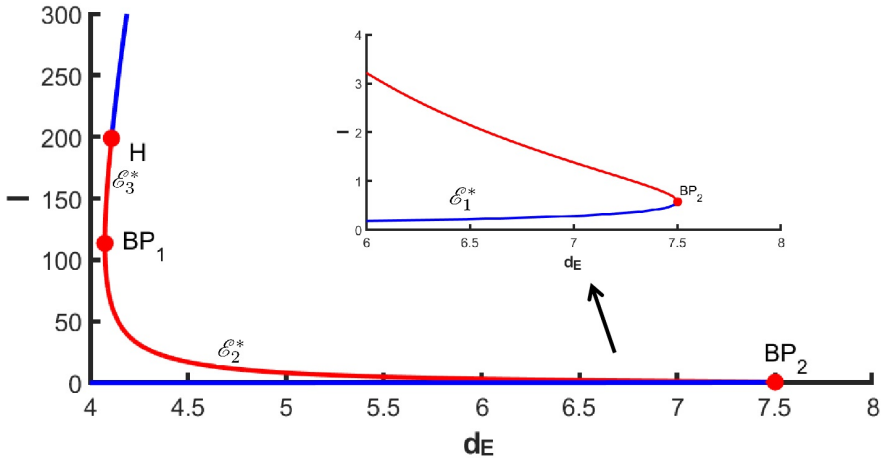

Figure 4: Bifurcation diagram with d_E as the bifurcation parameter. The value of m is chosen to be $m=0.42$. All other parameter values are listed in Table 1. BP denotes branch point and H denotes Hopf bifurcation point. Blue lines represent stable equilibrium, while red lines represent unstable equilibrium. The numerical simulation shows two branch points and Hopf bifurcation point at $d_E^{BP_1}=4.075, d_E^H=4.109$, and $d_E^{BP_2}=7.501$, respectively, as d_E increases. The first Lyapunov coefficients of system (3.1) at $d_E=d_E^H$ is 1.994×10^{-4}.

points $(d_E^{BP,1}, d_E^{BP,2})$ and one Hopf bifurcation point (d_E^H). When $d_E < d_E^{BP,1}$, the unique positive equilibrium $\mathscr{E}_1^*$ is locally asymptotically stable. If $d_E^{BP,1} < d_E < d_E^{BP,2}$, system (3.1) exhibits three positive equilibria $\mathscr{E}_1^*$, $\mathscr{E}_2^*$ and $\mathscr{E}_3^*$. The equilibrium $\mathscr{E}_1^*$ is stable, while $\mathscr{E}_2^*$ is unstable. A subcritical Hopf bifurcation, characterized by a positive first Lyapunov coefficient (1.994×10^{-4}), occurs at $\mathscr{E}_3^*$ when $d_E=d_E^H$. The equilibrium is stable for $d_E^H<d_E$ but unstable for $d_E<d_E^H$, with an unstable limit cycle emerging as d_E passes through d_E^H. For $d_E^{BP,2}<d_E$, system (3.1) has a unique positive equilibrium $\mathscr{E}_3^*$, which is locally asymptotically stable. These dynamical behaviors are illustrated in Fig. 6.

To further explore the complex dynamics of system (3.1), simulations are conducted for various values of parameter m, with the resulting behaviors illustrated in Fig. 5. The parameter values used in Figs. 5(a)-5(e) are $m=0.27, 0.35, 0.65, 0.6621$, and 0.68, respectively, with all other parameters being the same as in Fig. 3. Fig. 5(a), where $m=0.27<m^{BP,2}$, shows that all solutions converge to the unique positive equilibrium

$$\mathscr{E}_3^*(T_3^*, I_3^*, E_3^*) = (8.4986\times10^5, 1.3544\times10^3, 0.4020).$$

In Fig. 5(b) where $m=0.35$, system (3.1) has three positive equilibria $\mathscr{E}_1^*$, $\mathscr{E}_2^*$, and $\mathscr{E}_3^*$, and we observe that solutions converge to either

$$\begin{aligned} &\mathscr{E}_1^*(T_1^*, I_1^*, E_1^*) = (9.9993\times10^5, 0.5104, 0.8695) \\ \text{or}\quad &\mathscr{E}_3^*(T_3^*, I_3^*, E_3^*) = (8.7466\times10^5, 1.0987\times10^3, 0.4025), \end{aligned}$$

depending on the initial conditions. When m increases to 0.65 (Fig. 5(c)), passing through $m^{BP,1}$, system (3.1) possesses two positive equilibria $\mathscr{E}_2^*$ and $\mathscr{E}_3^*$. Here, solutions converge

to either the positive equilibrium

$$\mathscr{E}_3^*(T_3^*, I_3^*, E_3^*) = (9.7215 \times 10^5, 219.6075, 0.4124)$$

or the boundary equilibrium

$$\mathscr{E}_0(T_0, I_0, E_0) = (10^6, 0, 0.6667),$$

contingent upon initial conditions. For $m = 0.6621$ (Fig. 5(d)), which is slightly greater than m^H, system (3.1) still exhibits two positive equilibria $\mathscr{E}_2^*$ and $\mathscr{E}_3^*$, but its dynamical behavior differs from those shown in Fig. 5(c). In Fig. 5(d), a stable periodic solution exists, and, depending on the initial conditions, solutions converge to either the periodic solution or the boundary equilibrium $\mathscr{E}_0$. When m exceeds $m^{BP,3}$ ($m = 0.68$, Fig. 5(e)), system (3.1) has no positive equilibrium, and all solutions converge to the boundary equilibrium $\mathscr{E}_0$.

Simulations investigating the influence of various values of parameter d_E on system (3.1) are also performed, with the resulting behaviors shown in Fig. 6. The d_E values for Figs. 6(a)-6(e) are 4,4.09,4.15,7.4, and 7.6, respectively. All other parameter values remain consistent with those in Fig. 4. In Fig. 6(a) where $d_E = 4 < d_E^{BP,1}$, system (3.1) has a unique positive equilibrium

$$\mathscr{E}_1^*(T_1^*, I_1^*, E_1^*) = (9.9999 \times 10^5, 0.1098, 0.7246),$$

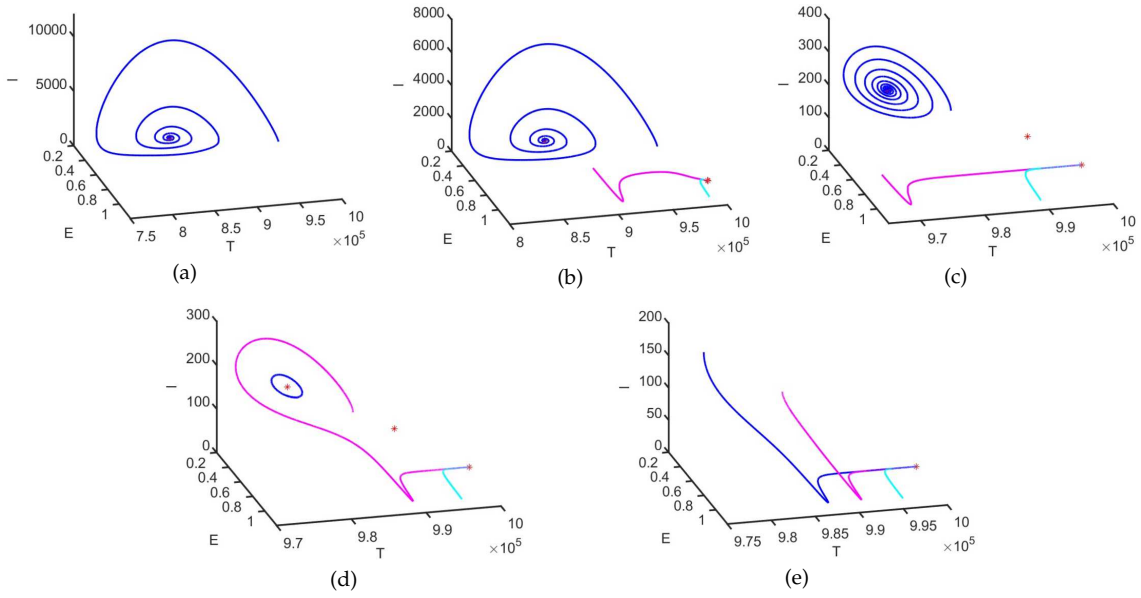

Figure 5: Numerical simulations (phase portraits) of system (3.1) for various m values chosen according to the bifurcation diagram in Fig. 3. Other parameter values are the same as in Fig. 3. (a) $m = 0.27$, (b) $m = 0.35$, (c) $m = 0.65$, (d) $m = 0.6621$, (e) $m = 0.68$. The red symbol $*$ represents the equilibria under the corresponding parameter conditions.

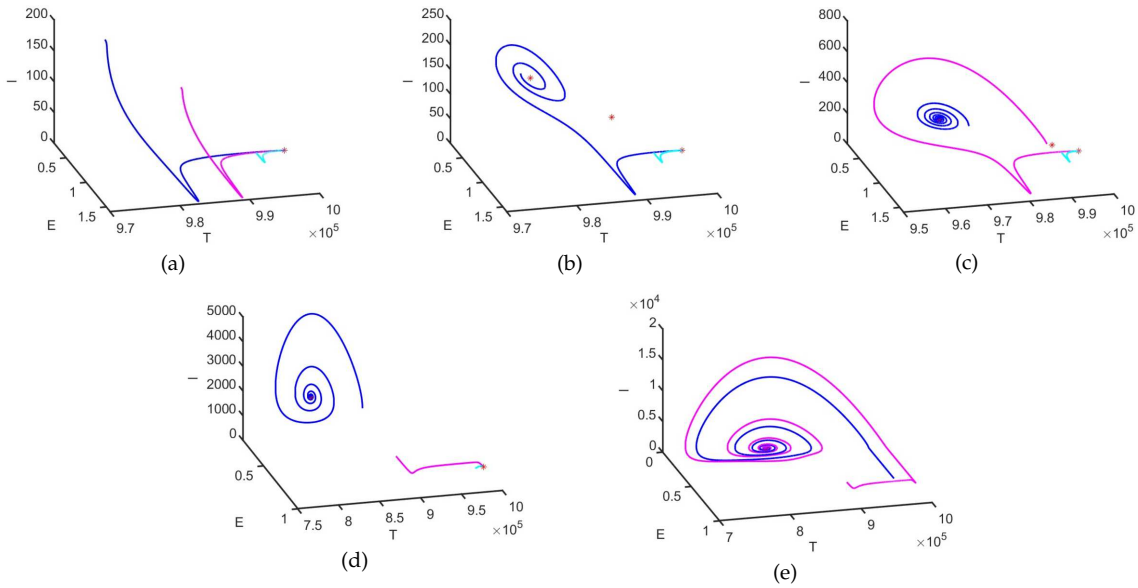

Figure 6: Numerical simulations (phase portraits) of system (3.1) for various d_E values chosen according to the bifurcation diagram in Fig. 4. Other parameter values are the same as in Fig. 4. (a) $d_E=4$, (b) $d_E=4.09$, (c) $d_E=4.15$, (d) $d_E=7.4$, (e) $d_E=7.6$. The red symbol $*$ represents the equilibria under the corresponding parameter conditions.

and all solutions converge to it. Fig. 6(b) shows that system (3.1) possesses three positive equilibria $\mathscr{E}_1^*$, $\mathscr{E}_2^*$, and $\mathscr{E}_3^*$, where all solutions converge to

$$\mathscr{E}_1^*(T_1^*,I_1^*,E_1^*)=(9.9999\times10^5,0.1120,0.7246)$$

since $d_E=4.09<d_E^H$. For $d_E=4.15$ (Fig. 6(c)), which is slightly greater than d_E^H, three positive equilibria persist, but the dynamical behavior differs from those shown in Fig. 6(b). In Fig. 6(c), an unstable periodic solution exists, and solutions converge to either

$$\begin{aligned}&\mathscr{E}_1^*(T_1^*,I_1^*,E_1^*)=(9.9999\times10^5,0.1134,0.7246)\\ \text{or}\quad&\mathscr{E}_3^*(T_3^*,I_3^*,E_3^*)=(9.6775\times10^5,255.4621,0.6245),\end{aligned}$$

depending on the initial conditions. When d_E increases to 7.4 (Fig. 6(d)), system (3.1) still exhibits three positive equilibria $\mathscr{E}_1^*$, $\mathscr{E}_2^*$, and $\mathscr{E}_3^*$, but no unstable periodic solution exists. Depending on the initial conditions, solutions converge to either

$$\begin{aligned}&\mathscr{E}_1^*(T_1^*,I_1^*,E_1^*)=(9.9994\times10^5,0.3905,0.7245)\\ \text{or}\quad&\mathscr{E}_3^*(T_3^*,I_3^*,E_3^*)=(8.3266\times10^5,1.5408\times10^3,0.2049).\end{aligned}$$

When d_E exceeds $d_E^{BP,2}$ ($d_E=7.6$, Fig. 6(e)), all solutions converge to the unique positive equilibrium

$$\mathscr{E}_3^*(T_3^*,I_3^*,E_3^*)=(8.3006\times10^5,1.5696\times10^3,0.1969).$$

To determine the key parameters governing infection control and immune function, we performed a sensitivity analysis of the steady-state infected cells (I) and effector cells (E) using partial rank correlation coefficients (PRCCs), as shown in Fig. 7. As indicated by $|PRCC| > 0.4$, parameter α shows the strongest positive impact on I, while m shows a significant negative effect. For E, parameters λ_E and b_E exhibit significant positive correlations, whereas d_E and μ exhibit significant negative correlations. Among these parameters, m represents the cytotoxic capacity of CD8$^+$ T cells against infected cells, and d_E reflects the threshold of proliferation impairment due to exhaustion. Both of these parameters are directly linked to the principal character of CD8$^+$ T cell exhaustion – reduced effector functions and decreased proliferative capacity. Therefore, it is reasonable to select these two parameters to characterize the dynamics of exhaustion and investigate their bifurcations.

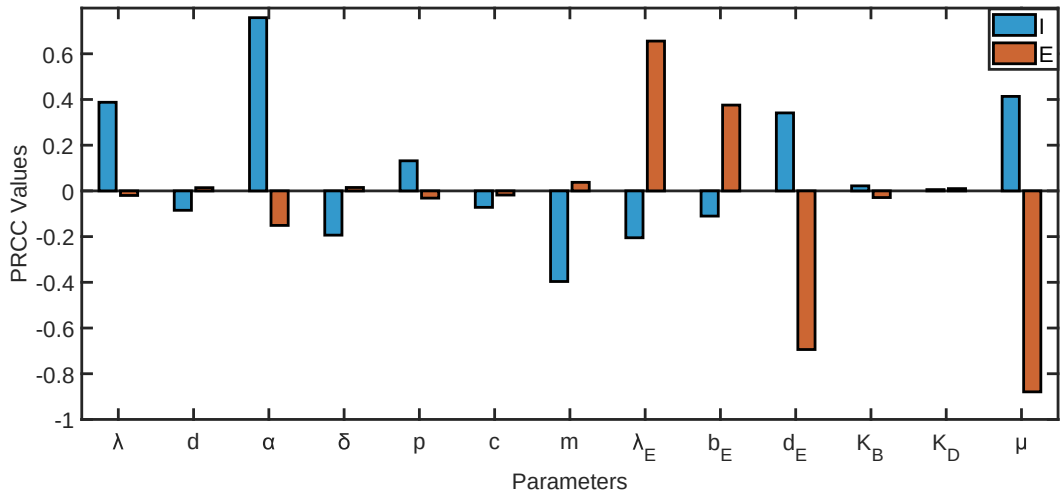

Figure 7: Parameter sensitivity analysis for the steady-state infected cells I (blue) and effector cells E (brown).

5 Tipping analysis of CD8$^+$ T cell exhaustion

In this section, we model the time-varying process of CD8$^+$ T cell exhaustion, and examine its impact on HIV infection dynamics through numerical simulations.

In chronic infections, the CD8$^+$ T cell progressively transition toward exhausted states, exhibiting escalating dysfunction. This ultimately leads to near-total differentiation into terminally exhausted CD8$^+$ T cells, resulting in virtual loss of antiviral functionality [4]. Here, we model this exhaustion process, denoted as $s(t)$, as a logistic growth function evolving from $s=0$ (onset of exhaustion) to $s=1$ (full exhaustion), given by

$$s(t) = \frac{1}{1+e^{-10rt+5}}.$$

The parameter r represents the progression rate of CD8$^+$ T cell exhaustion. Therefore, $1/r$ represents the time required for exhaustion to develop. Clinically, HIV infection progressors is categorized into three primary types based on disease progression rates [26]:

(1) rapid progressors who develop AIDS within 3 years of infection, potentially within less than one year [31];
(2) typical progressors who develop AIDS slowly, 3 to 10 years after seroconversion;
(3) long-term non-progressors who show no disease progression for at least 10 years.

Accordingly, we simulate CD8$^+$ T cell exhaustion durations aligned with these categories: 400 days (rapid progressors), 2400 days (typical progressors), and 4000 days (long-term non-progressors).

In absence of detailed information about the impact of exhaustion level on CD8$^+$ T cell functions (killing, expansion), we assume all these functions to be equally reduced with the level of CD8$^+$ T cell exhaustion [6]. Thus, the effector cell killing rate $m(s(t))$ and the saturation of immune impairment coefficient $d_E(s(t))$ are modeled as linear functions of the CD8$^+$ T cell exhaustion process $s(t)$:

$$m(s(t)) = (m_{end} - m_{start})s(t) + m_{start},$$
$$d_E(s(t)) = (d_{end} - d_{start})s(t) + d_{start}.$$

Here, m_{strat} and d_{start} denote the values of $m(s(t))$ and $d_E(s(t))$ at the onset of CD8$^+$ T cell exhaustion ($s=0$), respectively. Following reference [13], we set $m_{start}=0.42$. Naturally, the saturation of immune impairment coefficient without exhaustion is set to zero, i.e. $d_{start}=0$. m_{end} and d_{end} represent the values of $m(s(t))$ and $d_E(s(t))$ at full CD8$^+$ T cell exhaustion ($s=1$), respectively. Based on $>70\%$ reduced cytotoxicity-associated cytokine expression in exhausted CD8$^+$ T cells [22,47], we choose $m_{end}=0.1$. Assuming equivalent steady-state viral loads at $m=0.1$ and $d_E=d_{end}$, the bifurcation analysis yields $d_{end}=13$.

After the acute HIV phase, viral load stabilizes at a low set-point. We posit this equilibrium represents both stabilized host dynamics and the onset of CD8$^+$ T cell exhaustion. Based on bifurcation analysis, we initialize simulations at stable low-viral-load equilibria corresponding to CD8$^+$ T cell exhaustion onset. For time-varying m studies, we use the equilibrium $(999980, 0.13, 0.73)$ at $m=0.42$ (other parameters match Fig. 3). For time-varying d_E studies, we use $(999990, 0.064, 0.72)$ at $d_E=0$ (other parameters match Fig. 4).

Our analysis first examines how variations in parameter m during CD8$^+$ T cell exhaustion influence HIV infection dynamics. The simulation results are presented in Fig. 8. Fig. 8(a) shows the viral load trajectories over time t under different disease progression rates. All trajectories initiate from a low viral load state. As the infection progresses (i.e. the parameter m decreases), a critical transition (tipping, [1, 2]) occurs for three curves, characterized by a sharp increase in growth rate that drives rapid viral expansion to high levels. The trajectories then converge to relatively high steady states after damped oscillations. This progression aligns with the clinically observed shift from asymptomatic infection to AIDS. These findings indicate that CD8$^+$ T cell exhaustion not only elevates

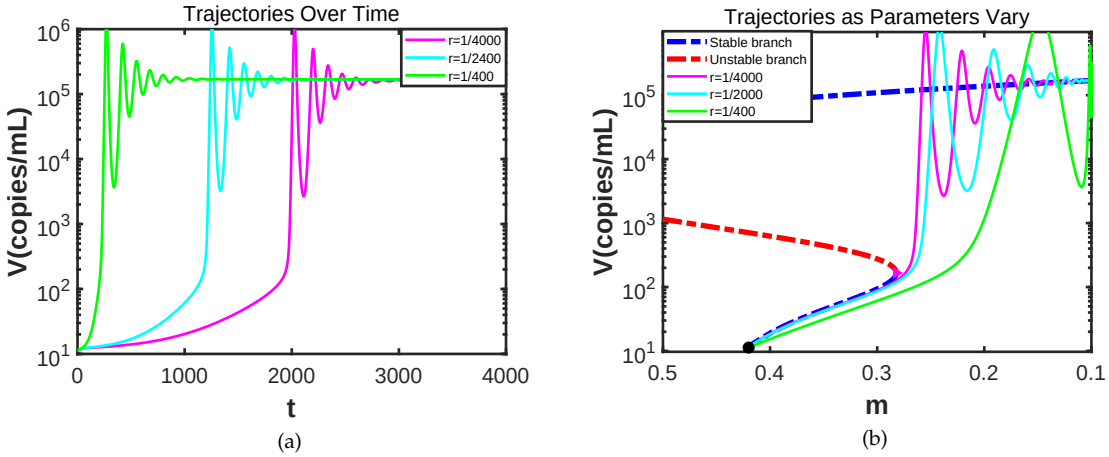

Figure 8: Viral dynamics under changes in parameter m induced by CD8$^+$ T cell exhaustion. (a) Time-evolution trajectories for different disease progression rates; (b) Corresponding trajectories as the parameter m changes. The magenta, cyan, and green solid lines correspond to long-term non-progressors ($r=1/4000$), typical progressors ($r=1/2400$), and rapid progressors ($r=1/400$), respectively. The thick dashed-dotted lines represent the bifurcation branches of the autonomous system (3.1), with blue indicating stable branches and red indicating unstable branches. The black dot is the starting point of the trajectories. The magenta triangle is the saddle-node bifurcation point corresponding to the point BP_2 in Fig. 3.

viral loads but also triggers a dynamical tipping point, leading to sustained high-level viremia. Moreover, a faster progression of CD8$^+$ T cell exhaustion (i.e. higher value of $1/r$) leads to earlier tipping points and lower viral load levels at the time of transition.

The underlying mechanisms behind the above-mentioned tipping phenomena require further investigation through bifurcation analysis of the autonomous system (3.1). Simulation results are shown in Fig. 8(b), which shows the viral load trajectories with different disease progression rates as parameter m changes. When $m>m^{BP_2}$, the autonomous system (3.1) possesses three positive equilibria: a low and a high viral load equilibrium, separated by an unstable equilibrium. As m decreases, the viral load of low viral load equilibrium increases gradually. In the non-autonomous system (2.4), trajectories originate within the basin of attraction of this low viral load state and follow its slowly rising stable branch. Once m crosses the saddle-node bifurcation point, the low viral load equilibrium and the unstable equilibrium collide and vanish, leaving a single high viral load equilibrium in the autonomous system. Deprived of the low viral load state, trajectories of the non-autonomous system rapidly converge toward the remaining high viral load state. The ascent rate surges sharply, driving the viral load rapidly to high levels. The trajectories then undergo damped oscillations before gradually converging to the high viral load stable branch. These behaviors exemplify B-tipping, a critical transition caused by the disappearance of a stable branch via bifurcation.

Our results show no evidence of R-tipping, where faster parameter progression alone would induce a critical transition without passing through a bifurcation point of the autonomous system. Furthermore, the bifurcation analysis of the autonomous system (3.1),

combined with Ashwin's theoretical framework [1], confirms that the chosen parameter pathway possesses forward basin stability. This theoretically precludes R-tipping under these conditions. While varying the progression rate ($1/r$) does not alter the qualitative trajectory patterns, it significantly affects their quantitative evolution. Specifically, a faster progression of CD8$^+$ T cell exhaustion leads to both lower viral load levels at equivalent exhaustion states (i.e. identical values of m) before critical transitions and higher exhaustion levels (i.e. smaller values of m) at the point of transition.

Next, we analyze the effect of changes in the parameter d_E during CD8$^+$ T cell exhaustion on HIV infection dynamics. Simulation results are presented in Fig. 9. Fig. 9 presents a pattern for parameter d_E similar to that in Fig. 8. For $d_E < d_E^{BP_2}$, the autonomous system (3.1) has three equilibria: stable low and high viral load states, separated by an unstable equilibrium. As d_E increases, the low viral load equilibrium rises gradually. Upon crossing the saddle-node bifurcation point, this stable state collides with the unstable equilibrium and annihilates, leaving only the high viral load equilibrium. Consequently, in the non-autonomous system (2.4), trajectories track the stable low viral load stable branch until the bifurcation, after which they converge rapidly toward the high viral load state. During which a B-tipping occurs, leading to rapid viral expansion; a faster progression rate of CD8$^+$ T cell exhaustion (i.e. higher $1/r$) results in an earlier tipping point, a lower viral load at equivalent exhaustion states (i.e. identical values of d_E), and a higher level of CD8$^+$ T cell exhaustion (i.e. a larger d_E) when the tipping occurs. However, compared to Fig. 8, the trajectories in Fig. 9 show slower viral load increases prior to B-tipping, lower viral loads at the tipping point, and longer time to reach the tipping point.

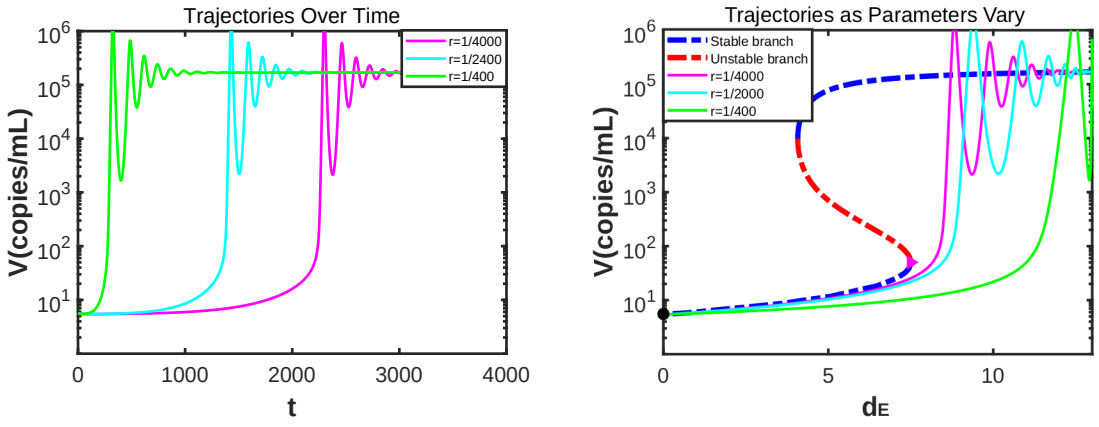

(a) (b)

Figure 9: Viral dynamics under changes in parameter d_E induced by CD8$^+$ T cell exhaustion. (a) Time-evolution trajectories for different disease progression rates; (b) Corresponding trajectories as the parameter d_E changes. The magenta, cyan, and green solid lines correspond to long-term non-progressors ($r = 1/4000$), typical progressors ($r = 1/2400$), and rapid progressors ($r = 1/400$), respectively. The thick dashed-dotted lines represent the bifurcation branches of the autonomous system (3.1), with blue indicating stable branches and red indicating unstable branches. The black dot is the starting point of the trajectories. The magenta triangle is the saddle-node bifurcation point corresponding to the point BP_2 in Fig. 4.

In summary, we simulate HIV infection dynamics with different $CD8^+$ T cell exhaustion progression rates (representing three types of infection progressors). The results show that:

(1) the increase in the level of $CD8^+$ T cell exhaustion drives an increase in viral load during HIV infection;

(2) the progression of $CD8^+$ T cell exhaustion triggers B-tipping, leading to a rapid viral surge;

(3) a faster rate of $CD8^+$ T cell exhaustion progression not only significantly accelerates progression from the asymptomatic phase to AIDS, but also results in a critical transition in the system where effector cell function is more impaired (smaller m) or proliferative potential is further reduced (larger d_E).

These results provide valuable insights into how $CD8^+$ T cell exhaustion impacts HIV infection dynamics.

6 Conclusion and discussion

$CD8^+$ T cell exhaustion is a key factor in HIV persistence. To explore its impact on virus-immune dynamics, we develop a novel time-varying parameter model of the $CD8^+$ T cell exhaustion process. Unlike prior mathematical models of HIV infection with exhaustion effects, which typically employ fixed parameters, our approach explicitly incorporates time-varying parameters to better capture actual biological progression. Building upon a constant-parameter model of HIV dynamics with CTL impairment, we focus on two key exhaustion features: weakened effector function and reduced proliferative capacity.

We apply the quasi-steady-state approximation to simplify the original model, resulting in a three-dimensional system with time-varying parameters. To understand the dynamics of the non-autonomous system (2.4), we first theoretically analyze the existence and local stability of equilibria in the corresponding autonomous system (3.1). Next, we explore the complex dynamics of system (3.1), focusing on parameters governing $CD8^+$ T cell exhaustion: the effector cell killing rate (m) and the saturation of immune impairment coefficient (d_E). Numerical simulations reveal distinct bifurcations: for m (one forward, two backward, and one supercritical Hopf bifurcations) and for d_E (one forward, one backward, and one subcritical Hopf bifurcations). Bifurcation analysis of both parameters also shows bistability. These theoretical and numerical results provide a solid foundation for analyzing the dynamics of the time-varying system (2.4).

Numerical simulations of system (2.4) assess how $CD8^+$ T cell exhaustion progression influences HIV infection dynamics. Figs. 8(a) and 9(a) demonstrate that this progression both increases viral load and triggers a critical transition, corresponding to the shift from asymptomatic infection to AIDS. Accelerated progression rates significantly shorten this

transition time. To further explore the underlying mechanisms, we combine the bifurcation behaviors of the autonomous system (3.1) with the dynamics of the non-autonomous system (2.4), as shown in Figs. 8(b) and 9(b). These figures indicate that $CD8^+$ T cell exhaustion drives key parameters (e.g. decreasing m or increasing d_E) across saddle-node bifurcation points, thereby triggering B-tipping. No evidence of R-tipping was observed. The rate of $CD8^+$ T cell exhaustion progression primarily determines the speed of disease progression and influences the severity of exhaustion at B-tipping: the faster the rate, the quicker the disease progresses, and the more severe the exhaustion state (i.e. smaller m or larger d_E) at which B-tipping occurs. Therefore, the extent of $CD8^+$ T cell exhaustion progression is the primary driver of viral growth and disease progression, while the rate only quantitatively modulates these processes. These findings suggest that, early intervention to slow exhaustion (i.e. reduce rate r) before B-tipping occurs could be more effective in prolonging the asymptomatic phase and improving long-term survival than intervention after severe exhaustion has developed.

This study has several limitations. First, to focus on the core impact of $CD8^+$ T cell exhaustion on HIV infection dynamics, our model omit several biologically elements: (i) latent infection, a major obstacle to HIV cure that evades both immune recognition and antiretroviral therapy [12]; (ii) $CD4^+$ T cell help, which is crucial for enhancing $CD8^+$ T cell function and limiting the progression toward exhaustion [3, 36]. Second, the multifaceted features of exhaustion is simplified into two consolidated parameters: effector cell kill rate and proliferative impairment. Third, we do not investigate N-tipping, as it requires consideration of external or internal noise effects.

Despite these simplifications, our framework provides a foundation for exploring more complex scenarios. Future studies could incorporate latent reservoirs and treatment to evaluate their interaction with exhaustion dynamics, following models such as [13]. Considering the role of $CD4^+$ T cells in immune responses [3, 24, 36], the model can be extended to include $CD4^+$ T cell help and dysfunction for a more integrated view of immune failure. The framework could also be extended to study exhaustion or exhaustion-like phenotypes in other immune cells, such as NK and B cells [7,11], following the multi-compartmental modeling approach for multiple cell types established in [28]. Furthermore, immunotherapeutic strategies to reverse T cell exhaustion, such as anti-PD-1/PD-L1 treatments [5,21], IL-15 activation [14], and epigenetic modulators [18,43], have shown promise in improving T cell function and antiviral capacity. Exploring how these interventions alter the system's trajectory, potentially redirecting it toward viral suppression and the tipping phenomenon involved, would be of significant theoretical and clinical value for optimizing combination strategies and improving patient outcomes.

In summary, this work establishes a time-varying model based on $CD8^+$ T cell exhaustion dynamics to analyze how $CD8^+$ T cell exhaustion influences HIV disease progression. We reveal that $CD8^+$ T cell exhaustion drives viral load increase and disease progression via the B-tipping mechanism, thereby providing a mathematical framework for understanding the role of $CD8^+$ T cell exhaustion in HIV infection. This offers novel methodological insights for developing therapeutic strategies against HIV.

Acknowledgments

The authors would like to thank the editor and the reviewers for their valuable suggestions and comments, which greatly improve the quality of the paper.

This work was supported by the National Natural Science Foundation of China (Grant No. 12201077), and by the fourth series of leading projects to introduce and cultivate innovative talents in Changzhou (Grant No. CQ20230111).

References

[1] P. Ashwin, C. Perryman, and S. Wieczorek, *Parameter shifts for nonautonomous systems in low dimension: Bifurcation- and rate-induced tipping*, Nonlinearity, 30:2185, 2017.

[2] P. Ashwin, S. Wieczorek, R. Vitolo, and P. Cox, *Tipping points in open systems: Bifurcation, noise-induced and rate-dependent examples in the climate system*, Philos. Trans. A Math. Phys. Eng. Sci., 370:1166–1184, 2012.

[3] R. D. Aubert et al., *Antigen-specific CD4 T-cell help rescues exhausted CD8 T cells during chronic viral infection*, Proc. Natl. Acad. Sci. USA, 108:21182–21187, 2011.

[4] A. Baessler and D. A. A. Vignali, *T cell exhaustion*, Annu. Rev. Immunol., 42:179–206, 2024.

[5] D. L. Barber, E. J. Wherry, D. Masopust, B. Zhu, J. P. Allison, A. H. Sharpe, G. J. Freeman, and R. Ahmed, *Restoring function in exhausted CD8 T cells during chronic viral infection*, Nature, 439:682–687, 2006.

[6] R. J. Beck, S. Sloot, H. Matsushita, K. Kakimi, and J. B. Beltman, *Mathematical modeling identifies LAG3 and HAVCR2 as biomarkers of T cell exhaustion in melanoma*, iScience, 26:106666, 2023.

[7] J. Bi and Z. Tian, *NK cell exhaustion*, Front. Immunol., 8:760, 2017.

[8] C. U. Blank et al., *Defining 'T cell exhaustion'*, Nat. Rev. Immunol., 19(11):665–674, 2019.

[9] S. Bonhoeffer, M. Rembiszewski, G. M. Ortiz, and D. F. Nixon, *Risks and benefits of structured antiretroviral drug therapy interruptions in HIV-1 infection*, AIDS, 14:2313–2322, 2000.

[10] Y. Cao, E. K. Cartwright, G. Silvestri, and A. S. Perelson, *$CD8^+$ lymphocyte control of SIV infection during antiretroviral therapy*, PLoS Pathog., 14:e1007350, 2018.

[11] K. S. Cashman et al., *Understanding and measuring human B-cell tolerance and its breakdown in autoimmune disease*, Immunol. Rev., 292:76–89, 2019.

[12] J. Chen, T. Zhou, Y. Zhang, S. Luo, H. Chen, D. Chen, C. Li, and W. Li, *The reservoir of latent HIV*, Front. Cell. Infect. Microbiol., 12:945956, 2022.

[13] J. M. Conway and A. S. Perelson, *Post-treatment control of HIV infection*, Proc. Natl. Acad. Sci. USA, 112:5467–5472, 2015.

[14] L. Darouni, F. T. Razavi, E. Yazdanpanah, N. Orooji, A. Shadab, A. Emami, H. Molavi, and D. Haghmorad, *Interleukin 15 and autoimmune disorders: Pathophysiology, therapeutic potential, and clinical implications*, Inflamm. Res., 74:141, 2025.

[15] Q. Deng, T. Guo, Z. Qiu, and L. Rong, *Modeling the effect of reactive oxygen species and CTL immune response on HIV dynamics*, Int. J. Bifurcat. Chaos, 31:2150203, 2021.

[16] C. Ding, Z. Qiu, and H. Zhu, *Multi-host transmission dynamics of schistosomiasis and its optimal control*, Math. Biosci. Eng., 12:983–1006, 2015.

[17] J. Drake and B. Griffen, *Early warning signals of extinction in deteriorating environments*, Nature, 467:456–459, 2010.

[18] H. E. Ghoneim et al., *De novo epigenetic programs inhibit PD-1 blockade-mediated T Cell rejuvenation*, Cell, 170:142–157, 2017.
[19] F. Graw and R. R. Regoes, *Predicting the impact of $CD8^+$ T cell polyfunctionality on HIV disease progression*, J. Virol., 88:10134–10145, 2014.
[20] T. Guo and Z. Qiu, *The effects of CTL immune response on HIV infection model with potent therapy, latently infected cells and cell-to-cell viral transmission*, Math. Biosci. Eng., 16:6822–6841, 2019.
[21] M. Hashimoto et al., *CD8 T cell exhaustion in chronic infection and cancer: Opportunities for interventions*, Annu. Rev. Med., 69:301–318, 2018.
[22] A. R. Hersperger et al., *Perforin expression directly ex vivo by HIV-specific $CD8^+$ T-cells is a correlate of HIV elite control*, PLoS Pathog., 6:e1000917, 2010.
[23] D. D. Ho, A. U. Neumann, A. S. Perelson, W. Chen, J. M. Leonard, and M. Markowitz, *Rapid turnover of plasma virions and CD4 lymphocytes in HIV-1 infection*, Nature, 373:123–126, 1995.
[24] G. Huang, Y. Takeuchi. and A. Korobeinikov, *HIV evolution and progression of the infection to AIDS*, J. Theor. Biol., 307:149–159, 2012.
[25] X. Jin et al., *Dramatic rise in plasma viremia after CD8(+) T cell exhaustion in simian immunodeficiency virus-infected macaques*, J. Exp. Med., 189:991–998, 1999.
[26] P. Kumar, *Long term non-progressor (LTNP) HIV infection*, Indian J. Med. Res., 138:291–293, 2013.
[27] T. M. Lenton, H. Held, E. Kriegler, J. W. Hall, W. Lucht, S. Rahmstorf, and H. J. Schellnhuber, *Tipping elements in the Earth's climate system*, Proc. Natl. Acad. Sci. USA, 105:1786–1793, 2008.
[28] Q. Li, F. Lu, and K. Wang, *Modeling of HIV-1 infection: Insights to the role of monocytes /macrophages, latently infected T4 cells, and HAART regimes*, PLoS One, 7:e46026, 2012.
[29] M. Markowitz, M. Louie, A. Hurley, E. Sun, M. Di Mascio, A. S. Perelson, and D. D. Ho, *A novel antiviral intervention results in more accurate assessment of human immunodeficiency virus type 1 repliation dynamics and T-cell decay in vivo*, J. Virol., 77:5037–5038, 2003.
[30] L. M. McLane, M. S. Abdel-Hakeem, and E. J. Wherry, *CD8 T cell exhaustion during chronic viral infection and cancer*, Annu. Rev. Immunol., 37:457–495, 2019.
[31] K. A. McLean, D. A. Holmes, B. A. Evans, L. McAlpine, R. Thorp, J. V. Parry, and M. G. Glase, *Rapid clinical and laboratory progression of HIV infection*, AIDS, 4:369–370, 1990.
[32] P. M. Ngina, R. M. Mbogo, and L. S. Luboobi, *Mathematical modelling of in-vivo dynamics of HIV subject to the influence of the $CD8^+$ T-cells*, Appl. Math., 8:1153–1179, 2017.
[33] T. Nishikawa and E. Ott, *Controlling systems that drift through a tipping point*, Chaos, 24:033107, 2014.
[34] M. A. Nowak and C. R. M. Bangham, *Population dynamics of immune responses to persistent viruses*, Science, 272:74–79, 1996.
[35] P. E. O'Keeffe and S. Wieczorek, *Tipping phenomena and points of no return in ecosystems: Beyond classical bifurcations*, SIAM J. Appl. Dyn. Syst., 19:2371–2402, 2020.
[36] F. Porichis et al., *Responsiveness of HIV-specific CD4 T cells to PD-1 blockade*, Blood, 118:965–974, 2011.
[37] R. R. Regoes, D. Wodarz, and M. A. Nowak, *Virus dynamics: The effect of target cell limitation and immune responses on virus evolution*, J. Theor. Biol., 191:451–462, 1998.
[38] L. Rong, Z. Feng, and A. S. Perelson, *Mathematical analysis of age-structured HIV-1 dynamics with combination antiretroviral therapy*, SIAM J. Appl. Math., 67:731–756, 2007.
[39] L. Rong and A. S. Perelson, *Modeling latently infected cell activation: Viral and latent reservoir persistence, and viral blips in HIV-infected patients on potent therapy*, PLoS Comput. Biol., 5:e1000533, 2009.
[40] M. Scheffer, E. H. van Nes, M. Holmgren, and T. Hughes, *Pulse-driven loss of top-down control:*

The critical-rate hypothesis, Ecosystems, 11:226–237, 2008.

[41] A. Schietinger and P. D. Greenberg, *Tolerance and exhaustion: Defining mechanisms of T cell dysfunction*, Trends Immunol., 35:51–60, 2014.

[42] J. E. Schmitz et al., *Control of viremia in simian immunodeficiency virus infection by $CD8^+$ lymphocytes*, Science, 283:857–860, 1999.

[43] M. Urbanek-Quaing et al., *Enhancing HBV-specific T cell responses through a combination of epigenetic modulation and immune checkpoint inhibition*, Hepatology, 82:739–754, 2025.

[44] A. Wang and M. Y. Li, *Viral dynamics of HIV-1 with CTL immune response*, Discrete Contin. Dyn. Syst. Ser. B, 26:2257–2272, 2021.

[45] K. Wang, W. Wang, and X. Liu, *Global stability in a viral infection model with lytic and nonlytic immune responses*, Comput. Math. Appl., 51:1593–1610, 2006.

[46] Z. Wang and X. Liu, *A chronic viral infection model with immune impairment*, J. Theor. Biol., 249:532–542, 2007.

[47] E. J. Wherry et al., *Molecular signature of $CD8^+$ T cell exhaustion during chronic viral infection*, Immunity, 27:670–684, 2007.

[48] E. J. Wherry, J. N. Blattman, K. Murali-Krishna, R. van der Most, and R. Ahmed, *Viral persistence alters CD8 T-cell immunodominance and tissue distribution and results in distinct stages of functional impairment*, J. Virol., 77:4911–4927, 2003.

[49] S. Wieczorek, P. Ashwin, C. M. Luke, and P. M. Cox, *Excitability in ramped systems: The compost-bomb instability*, Proc. R. Soc. A: Math. Phys. Eng. Sci., 467:1243–1269, 2011.

[50] World Health Organization, *HIV and AIDS: Key facts*, 2025. `https://www.who.int/zh/news-room/fact-sheets/detail/hiv-aids`

[51] A. J. Zajac, J. N. Blattman, K. Murali-Krishna, D. J. Sourdive, M. Suresh, J. D. Altman, and R. Ahmed, *Viral immune evasion due to persistence of activated T cells without effector function*, J. Exp. Med., 188:2205–2213, 1998.

[52] W. Zhang and L. A. Ellingson, *Detecting and resetting tipping points to create more HIV post-treatment controllers with bifurcation and sensitivity analysis*, SIAM J. Appl. Math., 84:S493–S514, 2024.